Modeling and Control of the Mitsubishi PA-10 Robot Arm Harmonic Drive System

Christopher W. Kennedy, *Student Member, IEEE,* and Jaydev P. Desai, *Associate Member, IEEE*

***Abstract*—The purpose of this paper is to present our results in developing a dynamic model of the Mitsubishi PA-10 robot arm for the purpose of low-velocity trajectory tracking using low-feedback gains. The PA-10 is ideal for precise manipulation tasks because of the backdrivability, precise positioning capabilities, and zero backlash afforded by its harmonic drive transmission (HDT). However, the compliance and oscillations inherent in harmonic drive systems, and the lack of any technical information on the internal dynamics of the transmission, make the development of an accurate dynamic model of the robot extremely challenging. The novelty of this research is therefore the development of a systematic algorithm to extract the model parameters of a harmonic drive transmission in the robot arm to facilitate model-based control. We have modeled all seven joints of the Mitsubishi PA-10, and we have done several experiments to identify the various parameters of the harmonic drive system. We conclude with a sample trajectory-tracking task that demonstrates our model-based controller for the Mitsubishi PA-10 robot arm.**

***Index Terms*—Harmonic drive transmission, Mitsubishi PA-10, model-based control.**

I. Introduction

ACCURATE modeling of the inherent dynamics of a robot manipulator is essential in many manipulation tasks. Through careful modeling, low-feedback gains can be used along with a feedforward model to accurately follow a desired trajectory for tasks requiring low-interaction forces while manipulating and interacting with objects in the environment.

The purpose of this paper is to present our results in developing a dynamic model of the Mitsubishi PA-10 robot arm for low-velocity applications such as surgical tool placement or teleoperated soft-tissue manipulation [1], [2]. Our goal is to develop a model-based controller that considers the inherent dynamics of the robot arm, such as the nonlinearities in its harmonic drive transmission (HDT) (for all joints), friction, and gravity effects. The PA-10 is ideal for precise manipulation tasks because of the backdrivability, accurate positioning capability, and zero backlash afforded by its HDT. However, the compliance and oscillations inherent in harmonic drive systems make the development of an accurate dynamic model of the robot extremely challenging. Additionally, because the robot is a commercial product offering limited access to the low-level subsystems, the challenge of modeling the robot is compounded because the only available tools for control are the input motor current and the motor shaft resolver readings for each joint. The novelty of this research is therefore the development of a systematic algorithm to extract the model parameters of a harmonic gear-driven transmission in the Mitsubishi PA-10 robot arm. This robot is significantly used in research laboratories worldwide [3]–[5], and we believe that the research presented in this paper for the Mitsubishi PA-10 robot arm is the first of its kind to address the transmission modeling and low-velocity, low-impedance implementation in a research environment. Modeling of robot dynamics for the purpose of trajectory tracking using low-feedback gains has been studied previously for the cable-driven whole arm manipulator (WAM) robot arm [6]. However, in that approach the transmission from the motor shaft to the output joint motion was through cable transmission. In our previous work [7], we presented the preliminary model for the elbow pitch joint (joint 4) of the Mitsubishi PA-10 robot arm. In this paper, we present the model for all seven joints and demonstrate its implementation through an end-effector trajectory-tracking experiment.

A substantial body of previous research exists in the area of modeling harmonic drive systems [8]–[10]. Tuttle [8] presented an excellent overview of modeling and parameter identification of harmonic drive systems and Kircanski and Goldenberg [9] provided a detailed analysis of the nonlinear behavior of harmonic gears due to compliance, friction, and hysteresis. Although these research efforts have provided significant insight into the physical phenomena that characterize harmonic drive behavior, all their experimental work has been performed on custom-designed, elaborate testbeds that allow direct measurement of many important system parameters such as compliance and kinematic transmission error. In addition, many control schemes for harmonic drive systems have relied on torque sensors mounted directly on the transmission components [11]–[13]. To our knowledge, no published work to date describes an efficient means of modeling, parameter identification, and control of the HDT in the Mitsubishi PA-10 robot arm. Previous work in modeling the Mitsubishi PA-10 robot arm includes classical modeling techniques using a rigid-body model [5] and static measurements of joint compliance [14], [15]. Our work is distinct from these previous works in that our model accounts for nonlinearities in the harmonic drive systems due to friction, kinematic error, and nonlinear stiffness behavior in the compliant elements in the gearing. There is also significant research in the area of controlling harmonic drive systems. A model-based approach is presented in [16]; however, this approach neglects kinematic error in the transmission. A number

Manuscript received January 17, 2004; revised July 10, 2004. This work was supported in part by National Science Foundation under Grant EIA-0312709, CAREER Award IIS 0133471, and the American Heart Association under Grant 0160368U. Recommended by Technical Editor M. Meng.

The authors are with the Program for Robotics, Intelligent Sensing, and Mechatronics (PRISM) Laboratory, Drexel University, Philadelphia, PA 19104 USA (e-mail: cwk@coe.drexel.edu; desai@coe.drexel.edu).

Digital Object Identifier 10.1109/TMECH.2005.848290

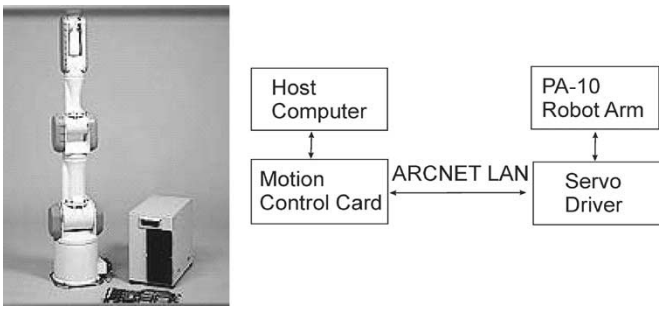

Fig. 1. Mitsubishi PA-10 robot arm with servo driver, and flowchart of Mitsubishi PA-10 four-layer control architecture.

of other control schemes have also been suggested, such as an H_∞ framework [17], [18] and kalman filtering [19].

The rest of this paper is organized as follows. In Section II, the Mitsubishi PA-10 system is described, including the control system architecture. In Section III, a brief overview of the HDT along with a model of harmonic gearing is presented, and in Section IV our methods for experimentally determining the necessary parameters for model-based control of the PA-10 robot arm are described. Section V details our experiments designed to verify the effectiveness of our model, Section VI presents a discussion of our experimental results, and finally in Section VII concluding remarks are presented.

II. The Mitsubishi PA-10 Robot Arm

The Mitsubishi PA-10 robot arm is a 7 degree-of-freedom robot arm with an open-control architecture and is manufactured by Mitsubishi Heavy Industries (see Fig. 1, our robot is model PA-10, serial number PA-10-4CE-0008). The four-layer control architecture is made up of the robot arm, servo controller, motion control card, and the upper control computer. A flow-chart for the control system is shown in Fig. 1. The host computer runs the QNX real-time operating system and we have been able to achieve communication rates of up to 700 Hz with the robot servo driver through the ARCNET (ARCNET is a token passing LAN protocol developed by Datapoint Corporation) communication card (model ARC-AT, manufactured by Toyomicrosystems Corp.) and custom-made software written in the C programming language.

The robot joints are actuated by three-phase AC servo motors and harmonic gear transmissions. The harmonic drive assemblies in the Mitsubishi PA-10 are manufactured by Harmonic Drive Systems Inc. (model CSF-32-50-2A-GR for joints 1 and 2, model CSF-32-50-2A-GR for joints 3 and 4, and CSF-32-50-2A-GR for joints 5, 6, and 7). Joint positions are measured through resolvers at the joint output axis, with a resolution of 0.000439° over ± 3 output revolutions.

Control of the robot can be achieved in either "velocity mode" or "torque mode." In velocity mode, the desired velocity for each joint is sent to the servo driver from the host computer. A high-gain digital PI feedback loop running at 1504 Hz on the servo driver controls the joint velocity. In torque mode the desired joint torque (in this case, the motor torque constant times the motor current, before conversion by three-phase), is sent to the servo driver. The expression for communicating a desired torque to the robot arm through the servo driver in this system is given by:

$$T_{\mathrm{m}} = k_{\mathrm{T}} * I = T_{\mathrm{d}} * \left(0.001 \ \frac{\mathrm{N \cdot m}}{\mathrm{digit}}\right) \tag{1}$$

where T_{m} is the motor torque, k_{T} is the motor torque constant, I is the motor current, and T_{d} is the desired torque written to the servo driver in the form of a two-byte integer.

III. Harmonic Drive Systems

Harmonic gears (also called strain-wave gearing) were developed by C. Walton Musser in the 1950s primarily for aerospace applications. They are compact, lightweight, and have torque transmission ratios between 30:1 and 320:1, making them ideal for robotics applications. Harmonic drives are composed of three components: the wave generator, the flexspline, and the circular spline. The wave generator is an elliptical ball-bearing assembly and is nested inside the flexspline. The teeth on the non-rigid flexspline and the rigid circular spline are in continuous engagement. Because the flexspline has two teeth fewer than the circular spline, one revolution of the input causes relative motion between the flexspline and the circular spline equal to two teeth. With the circular spline rotationally fixed, the flexspline rotates in the opposite direction to the input at a reduction ratio equal to one-half the number of teeth on the flexspline. The displacement, velocity, and torque relationships between the transmission elements in the ideal case are therefore given by

$$\theta_{\mathrm{wg}} = (N+1)\theta_{\mathrm{cs}} - N\theta_{\mathrm{fs}} \tag{2}$$

$$\omega_{\mathrm{wg}} = (N+1)\omega_{\mathrm{cs}} - N\omega_{\mathrm{fs}} \tag{3}$$

$$T_{\mathrm{wg}} = \frac{1}{(N+1)} T_{\mathrm{cs}} = \frac{1}{N} T_{\mathrm{fs}} \tag{4}$$

where N is the transmission ratio, θ is the angle, ω is the angular velocity, T is the torque, and subscripts "fs", "cs," and "wg" refer to the flexspline, circular spline, and wave generator, respectively. In general, either the flexspline or the circular spline can be fixed. However, in our robot the circular spline is fixed while the flexspline rotates with the joint. The flexibility inherent in the HDT provides advantages such as zero backlash due to natural preloading. However, there are also several disadvantages such as nonlinearity due to friction, alignment error of the components, and transmission losses due to the compliance in the system. All these were found to be critical in the modeling of the Mitsubishi PA-10 robot arm. In the following sections, we will describe in detail our methodology to estimate and model: 1) velocity-dependent and position-dependent friction; 2) torsional stiffness; and 3) gravity effects.

IV. Modeling

Parameter identification of the Mitsubishi PA-10 robot arm was carried out using the system and control architecture described above. Although the system did allow us to control the

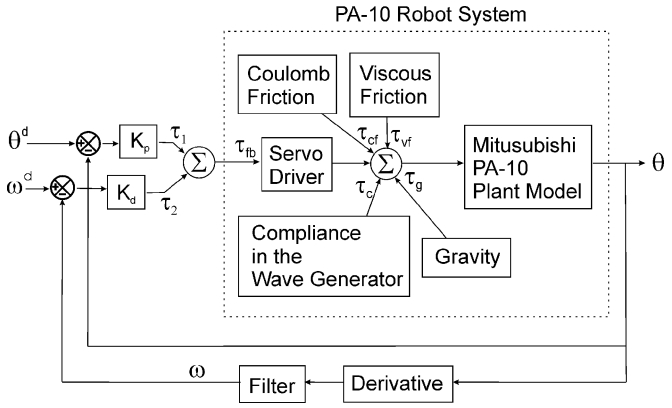

Fig. 2. The proposed control system includes models of friction, gravity, and nonlinear stiffness of the wave generator.

motor torque of each joint, we preferred to conduct our experiments in velocity mode when possible. The use of velocity mode allowed for better high-gain trajectory tracking because of the increased feedback-loop rate and the use of the tuned proportional-integral controller provided by Mitsubishi. Therefore, velocity mode experiments provided a better means of using feedback torque as a disturbance estimator for identifying model parameters. The torque data for the joints in velocity mode were communicated from the servo driver to the host computer as calculated by (1).

In this paper, we present our experimental results for all seven joints of the Mitsubishi PA-10 robot arm in tabular format, along with representative plots of the results of joint 2. We chose joint 2 as the representative joint because it is strongly affected by friction, gravity, and nonlinear stiffness effects in the HDT.

A. Harmonic Drive Model

We consider the model of the harmonic drive to be composed of friction, gravity, and stiffness. Because we are primarily concerned with low-velocity and low-acceleration applications (such as in surgery), the only torque components from the robot arm dynamics will be the gravitational torque, friction torque, and stiffness in the HDT. The nonlinear expression for torque transmission in harmonic drives is thus given by

$$T_{\rm in}N = T_{\rm cf}(\theta) + T_{\rm vf}(\dot{\theta}) + T_{\rm g}(\theta) + T_{\rm c}(T_{\rm cf}, T_{\rm vf}, T_{\rm g}) \qquad (5)$$

where $T_{\rm in}$ is the input torque, N is the transmission ratio (N is 50 for all joints), $T_{\rm cf}$ is the coulomb friction, $T_{\rm vf}$ is the velocity-dependent friction torque, $T_{\rm g}$ is the gravity torque, and $T_{\rm c}$ is the torque used to deform the wave generator. A schematic for the proposed control system is shown in Fig. 2. The following sections describe in detail the estimation and modeling procedure for the various terms on the right-hand side of (5).

B. Friction

Our approach for modeling friction in the Mitsubishi PA-10 robot arm was similar to the approach described by Armstrong-Helouvry in [20]. In Armstrong-Helouvry's work, friction was modeled as a function of both velocity and position. The velocity-dependent friction model was found by fitting experimental friction data to several mathematical models, and statistical analysis was performed to determine the best mathematical model to describe the velocity-dependent friction. Armstrong-Helouvry used three methods for gathering friction data for a given velocity in the robot joint: 1) high-gain closed-loop control to maintain a constant velocity (the mean torque for tracking the velocity was taken to be the value of friction for that velocity); 2) open-loop velocity tracking using a simple dynamic model for the joint (the mean velocities for these trajectories were used to determine the friction-velocity relationship); and 3) compliant motion control to gather friction data at slow velocities. In our work, we have used the velocity mode control method, i.e., high-gain closed-loop control, because we were able to achieve good velocity tracking even at very low velocities (<0.01 rad/s). To model position-dependant friction, Armstrong-Helouvry collected breakaway torque data for positions across the range of motion of the joint and fed-forward interpolated breakaway data in his controller. In our experiments with the Mitsubishi PA-10 robot arm, we found that the torque required to maintain a very slow velocity (0.01 rad/s) provided nearly identical results with the breakaway torque approach followed by Armstrong-Helouvry. Therefore, we modeled the position-dependent friction in the Mitsubishi PA-10 robot arm as the torque required to maintain a velocity of 0.01 rad/s and we fed-forward this torque in the form of a lookup table. The following sections describe in detail our methodology for modeling both velocity-dependent friction and position-dependent friction in the Mitsubishi PA-10.

1) Velocity-Dependent Friction: Many models for friction in mechanisms exist [20]. Friction in harmonic drive systems occurs primarily at the gear-tooth interface and is influenced by factors such as wave generator orientation, velocity, and resonance vibration [21]. Tuttle [8] modeled friction for harmonic drives as a combination of coulomb friction and viscous friction, with the viscous term represented by a cubic polynomial. In his model, viscous friction behaved linearly at lower velocities and decreased at high velocity. Taghirad [10], however, found a linear relationship at high velocities and modeled low velocities by using a standard Stribeck curve with negative Stribeck coefficients.

To determine the friction–velocity relationship for the joints of the PA-10 robot arm, each joint of the robot was commanded to move at a constant velocity and the mean torque required to maintain the velocity was taken to be the friction for that value of velocity. These experiments were performed with the robot in velocity mode. To characterize the friction behavior at low velocity, data for velocities between 0.02 and 0.1 rad/s were collected in 0.02 rad/s increments and between 0.1 and 0.4 rad/s in 0.1 rad/s increments. Five trials were performed for each velocity value in both the positive and negative directions, for a total of 80 measurements per joint. For joints 2, 4, and 6 (which are influenced by gravity), the robot was mounted on the wall as shown in Fig. 3 to negate the effect of gravity. Data for joints 1, 3, 5, and 7 were collected with all the joints in the vertical position. After collecting data for all seven joints, we fit three different friction models using least-squares techniques.

TABLE I
DATA FOR THREE DIFFERENT MODELS OF VELOCITY-DEPENDENT FRICTION INCLUDING THE VISCOUS FRICTION MODEL, THE CUBIC MODEL, AND THE STRIBECK MODEL

Joint	Viscous model			Cubic model			Stribeck model		
	Model DOF	Residual variance, weighted	MSE per DOF	Model DOF	Residual variance, weighted	MSE per DOF	Model DOF	Residual variance, weighted	MSE per DOF
1	2	12.1404	4.0351	4	1.8519	1.9260	4	2.2302	2.1151
2	2	22.2687	6.5672	4	2.8653	2.4327	4	5.2306	3.6153
3	2	114.6001	29.6500	4	16.9548	9.4774	4	2.7248	2.3624
4	2	415.8925	104.9730	4	0.1180	1.0590	4	1.4081	1.7041
5	2	147.7424	37.9256	4	33.4068	17.7034	4	0.6805	1.3403
6	2	1.7577	1.4394	4	0.4013	1.2006	4	0.5518	1.2759
7	2	741.2334	186.3080	4	1.9773	1.9887	4	0.7370	1.3685

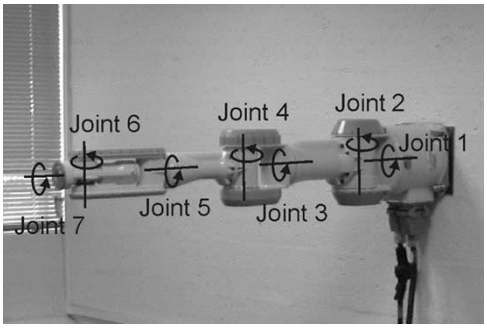

Fig. 3. Robot configuration for constant velocity experiments.

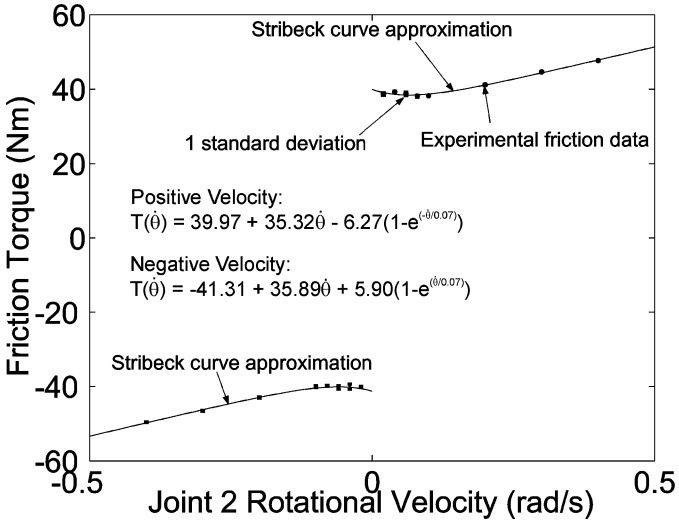

Fig. 4. Representative plot of velocity-dependent friction for joint 2. The friction data along with the best-fit Stribeck curve are shown above for positive and negative velocities.

The three models tested were 1) the kinetic plus viscous friction model, 2) the cubic polynomial model, and 3) the Stribeck curve model. The results of this analysis are shown in Table I. We compared different friction models based on their ability to fit experimental data. The results presented in Table I are the weighted residual variance and the mean-squared error (MSE) per degree-of-freedom (DOF) for each model after being fit to the collected experimental data. The weighted residual variance for the kinetic plus viscous friction model is given by [20]:

$$\sigma^2 = \tilde{\boldsymbol{T}}^T W \tilde{\boldsymbol{T}} \tag{6}$$

where $\tilde{\boldsymbol{T}}$ is torque not predicted by the model, and W is the covariance matrix of the data vector $\boldsymbol{T}$ (vector of applied torques). The weighted residual variance represents the mean number of standard deviations by which the model misses each datum, and the MSE is a measure of the residual variance per DOF of the model.

In our experiments with the Mitsubishi PA-10 robot arm, we have observed several different relationships between friction torque and velocity as observed from the data in Table I. Although the joints vary in their behavior at low velocity, the friction torque versus velocity relationship for all seven joints could be approximated by a viscous friction model at higher velocities. Based on our observations, we concluded that no single-friction model was appropriate to describe the friction behavior in all joints of our robot. However, the Stribeck model provided a reasonably good approximation for the friction torque in all seven joints of the Mitsubishi PA-10 robot arm that we have modeled. Although the residual variance for the cubic model is smaller than the Stribeck model for some of the robot's joints, the Stribeck model had the advantage of approximating friction as linear at higher velocities and exponential at low velocities (which was consistent with our experimental observations). The expression for this model is given by:

$$T_{\mathrm{vf}}(\dot{\theta}) = F_{\mathrm{o}}\,\mathrm{sgn}(\dot{\theta}) + F_{\mathrm{v}}\dot{\theta} + F_{\mathrm{s}}(1 - \exp[-\dot{\theta}/V_{\mathrm{c}}]) \tag{7}$$

where T_{vf} is the viscous friction torque, $F_{\mathrm{o}}, F_{\mathrm{v}}, F_{\mathrm{s}}$, and $\mathrm{V_c}$ are the Stribeck coefficients, and $\dot{\theta}$ is the rotational velocity. The best-fit approximation of experimental data by a Stribeck curve is shown in Fig. 4 for both positive and negative velocities for joint 2. Fig. 4 shows the Stribeck curve and the experimental data with error bars representing one standard deviation, and Table II gives the Stribeck coefficients for all seven joints. Joint 1 had a nearly linear relationship between friction torque and velocity, joints 2 through 6 exhibited varying degrees of decreasing viscous friction with increasing velocity, and joint 7 exhibited behavior similar to Taghirad's model with negative Stribeck coefficients at low velocity. The velocity in Fig. 4 is the output joint velocity (flexspline velocity), which is given by (3). This approach was used for all the velocity and position calculations in this paper. The calculated parameters for the Stribeck curve describing friction torque in both the positive and negative direction is shown in Table II for all of the joints.

TABLE II
COEFFICIENTS FOR STRIBECK CURVE DESCRIBING LOW-VELOCITY FRICTION BEHAVIOR FOR SEVEN JOINTS IN BOTH THE POSITIVE AND NEGATIVE DIRECTIONS

	Positive direction				Negative direction			
Joint	F_0	F_v	F_s	V_c	F_0	F_v	F_s	V_c
1	34.9647	29.7153	2.8103	0.3376	36.7050	26.4796	−2.2885	−0.6172
2	39.9709	35.3200	6.2713	0.0685	41.3113	35.8947	−5.9018	−0.0709
3	18.3053	17.6413	2.2282	0.0430	18.7327	17.8371	−2.7240	−0.0405
4	30.4416	28.5552	19.7181	0.3278	30.6897	29.4670	−21.7854	−0.3676
5	3.7145	0.7493	1.0792	0.0386	4.1271	0.7919	−1.3756	−0.0393
6	5.5090	0.5859	0.9983	0.0126	5.7954	0.5711	−0.9967	−0.0135
7	2.2980	0.6062	−1.1803	0.0759	2.3027	0.6836	1.1470	−0.0690

2) Position-Dependent Friction: Friction in the HDT is strongly position dependent because of kinematic error in the transmission. Harmonic drives display kinematic error that causes the torque transmission characteristics of the drive to deviate from the ideal transmission model. This error is caused by a number of factors, such as tooth-placement errors on both the circular spline and flexspline, out-of-roundness in the three transmission components, and misalignment during assembly [8]. The resulting error signature can display frequency components at two cycles per wave generator revolution and several subsequent harmonics. Based on the above, the error function including two harmonics of wave generator rotation can be expressed as

$$\theta_{\mathrm{erfn}} = A_1 \sin(\theta_{\mathrm{wg}} + \varphi_1) + \mathrm{A}_2 \sin(2\theta_{\mathrm{wg}} + \varphi_2) \qquad (8)$$

where θ_{erfn} is the error function, A_i are the amplitudes of the sinusoids, φ_i is the phase shift, and θ_{wg} is the wave generator position. This expression is of limited use in our case, because it is not possible to measure the output axis rotation. The amplitudes in (8) are therefore impossible to accurately determine for our robot. Although kinematic error has a significant effect on the torque transmission characteristics of HDTs, we found that compensating for coulomb friction using the torque required to maintain slow velocity (0.01 rad/s) eliminated almost all the effects of kinematic error at low velocity. Therefore, we neglected the effect of kinematic error in the feedforward implementation of our model.

Because of the position dependence of friction in the HDT, we model coulomb friction as the torque required to maintain a very slow velocity over the entire range of motion of the joint. To quantify the position-dependent component of the HDT friction, we performed a fast Fourier transform (FFT) to determine the frequency content of the coulomb friction torque (the torque required to maintain a velocity of 0.01 rad/s acquired in velocity mode). Our FFT results revealed two dominant frequencies in our position-dependent friction data. These results agree with the findings of Tuttle [8], where the kinematic error was found to be approximated well by using the first two frequencies of the kinematic error function [(8)]. In Fig. 5, a fit of the FFT results with the zero-mean experimental friction torque is shown for joint 2.

As can be observed from the plot in Fig. 5, the FFT results provide a good approximation of the position-dependent friction torque. The parameters for position-dependent friction torque are presented in Table III for all seven joints. These results are presented only to demonstrate the nature of position-dependent friction in the HDT. In our control scheme, the torque required to maintain a velocity of 0.01 rad/s was fed forward in the form of a lookup table to eliminate the errors in estimating the magnitudes and phase shifts of the periodic components with the FFT. The zero-mean position-dependent friction torque similar to the data in Table III along with the velocity-dependent friction torque given by the data in Table II completely characterizes the HDT friction in our Mitsubishi PA-10 robot arm.

TABLE III
PARAMETERS FOR PERIODIC FRICTION TORQUE FOR SEVEN JOINTS INCLUDING TWO HARMONICS OF WAVE GENERATOR ROTATION

Joint	f_1	A_1	φ_1	f_2	A_2	φ_2
1	15.87	7.50	2.30	47.60	5.05	12.80
2	47.60	6.00	-1.50	310.50	2.50	-6.90
3	39.65	0.70	0.10	239.20	0.55	5.50
4	39.65	5.00	-3.15	262.50	0.10	3.98
5	23.80	0.50	4.95	95.80	0.40	7.50
6	23.80	0.10	-1.50	95.80	0.50	5.50
7	23.80	0.10	-1.00	95.80	0.50	2.50

C. Gravity Compensation

The parameters used for gravity compensation in our model were taken from the catalog values for the masses and the center-of-mass locations for the robot links. In much of the previous research regarding modeling of robot manipulators, the link masses were determined through least-squares-based techniques. In our case, this approach would have been extremely difficult to implement because of limitations of hardware access for the Mitsubishi PA-10 robot arm. Specifically, the kinematic error and compliance in the HDT could not be directly measured without an output axis resolver measurement, which was not present in the Mitsubishi PA-10 control architecture. Therefore, any attempt to measure the system parameters through least-squares techniques would have been error prone because of the lack of sufficient information to fully characterize the state of the system.

The effect of gravity was significant only for joints 2 through 6 when the robot was mounted on a pedestal. A schematic of the Mitsubishi PA-10 robot arm along with the location of the centers of gravity (COG) is shown in Fig. 6.

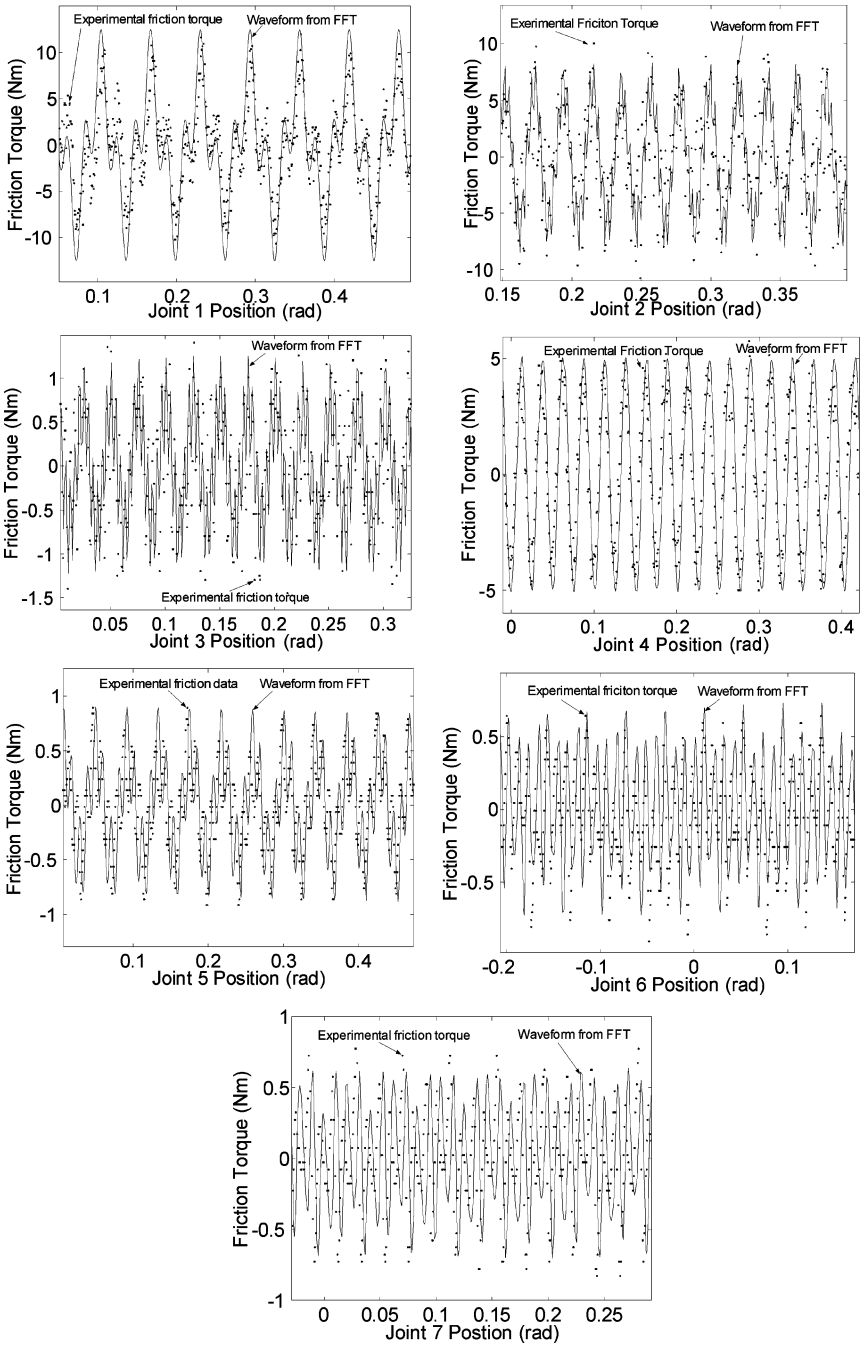

Fig. 5. Comparison between experimental friction torque and FFT results for the periodic friction torque.

The gravity torques for joints 2 through 6 are given by

$$\begin{aligned}\tau_{2g} = {} & m_2 g l_{c2}(c_2) + m_4 g \left[l_2(c_2 s_2) + l_{c4} \left(s_2 s_3 s_4 \right.\right. \\ & \left.\left. + \; c_2^2 c_3 s_4 + c_2 s_2 c_4 \right) \right] \\ & + m_6 g \left[l_2(c_2 s_2) + l_4 \left(s_2 s_3 s_4 + c_2^2 c_3 s_4 \right) \right. \\ & + l_{c6} \left(s_2 s_3 c_4 c_5 s_6 + s_2 c_3 s_5 s_6 + s_2 s_3 s_4 c_6 + c_2^2 c_3 c_4 c_5 s_6 \right. \\ & \left.\left. - \; c_2 s_2 s_4 c_5 s_6 - c_2^2 s_3 s_5 s_6 + c_2^2 c_3 s_4 c_6 + c_2 s_2 c_4 c_6 \right) \right] \quad (9)\end{aligned}$$

$$\begin{aligned}\tau_{3g} = {} & m_4 g [l_{c4} s_2 c_3 (c_4 + s_3 s_4)] + m_6 g \left[l_4 s_2 (c_3 c_4 + s_3 c_3 s_4) \right. \\ & + l_{c6} s_2 \left(c_3 c_4 c_6 - c_3 s_4 c_5 s_6 + s_3 c_3 c_4 c_5 s_6 \right. \\ & \left.\left. - \; s_5 s_6 + c_3^2 s_5 s_6 + s_3 c_3 s_4 c_6 \right) \right] \quad (10)\end{aligned}$$

$$\begin{aligned}\tau_{4g} = {} & m_4 g [l_{c4} s_4 (s_2 c_3 s_4 - c_2 c_4)] \\ & + m_6 g \left[l_4 \left(s_2 c_3 c_4^2 + c_2 c_4 s_4 \right) + l_{c6} \left(s_2 c_3 c_4 s_5 s_6 \right. \right. \\ & + c_2 s_4 s_5 s_6 - s_2 c_3 s_4 c_4 c_5 s_6 + c_2 c_4^2 c_5 s_6 - s_2 c_3 c_6 \\ & \left.\left. + \; s_2 c_3 c_4^2 c_6 + c_2 c_4 s_4 c_6 \right) \right] \quad (11)\end{aligned}$$

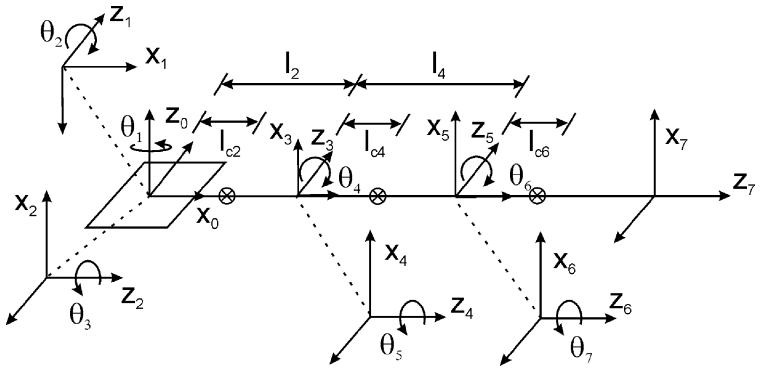

Fig. 6. Schematic of the PA-10 robot arm for gravity compensation.

TABLE IV
CATALOG VALUES FOR GRAVITY COMPENSATION PARAMETERS

l_2 = 0.45 m	l_{c2} = 0.32 m	m_2 = 9.86 kg
l_4 = 0.50 m	l_{c4} = 0.17 m	m_4 = 2.18 kg
-	l_{c6} = -0.09 m	m_6 = 4.34 kg

$$\tau_{5g} = m_6 g[l_{c6} s_6 (s_2 c_3 c_4 s_5 + c_2 s_4 s_5 + s_2 s_3 c_5)] \quad (12)$$

$$\tau_{6g} = m_6 g[l_{c6} s_6 (s_2 c_3 c_4 c_5 s_6 + c_2 s_4 c_5 s_6 - s_2 s_3 s_5 s_6 + s_2 c_3 s_4 c_6 - c_2 c_4 c_6)] \quad (13)$$

where $s_i = \sin(\theta_i)$, $c_i = \cos(\theta_i)$, and τ_{ig} = the gravity torque for joint i.

The catalog values for the necessary parameters for gravity compensation are shown in Table IV.

D. Estimation and Modeling of Nonlinear Stiffness

Harmonic drives exhibit significant compliance when externally loaded. This is apparently due to deformation of the wave generator [21]. Experimental tests in [8]–[10] indicate that stiffness in harmonic drives increases with increasing load. According to Nye and Kraml, this is due to an increase in gear-tooth contact area with increasing loads. In addition, harmonic drives display a behavior known as "soft wind-up" which is characterized by very low stiffness at low applied loads [21]. In this research, we assumed that all compliance in the Mitsubishi PA-10 robot arm system was due to deformation of the compliant elements of the harmonic drive system. This assumption was supported by our previous work [7] in which the compliance of the robot was shown to display a hysteresis behavior very similar to that reported by the harmonic drive manufacturer for the gears, and by previous work by Khalil [14] in which the links of the Mitsubishi PA-10 robot arm were found to be too stiff to accurately determine their stiffness parameters.

Our experimental tests on the Mitsubishi PA-10 robot arm revealed that wave generator compliance has a significant effect on the robot arm dynamics. The effect of the nonlinear stiffness profile of the wave generator was prevalent when the load on the wave generator was below a critical point where a significant decrease in stiffness occurred. Measuring stiffness presented a unique challenge in this case. Stiffness measurements of harmonic drive systems are typically made by fixing the wave generator position and observing the resulting torsion angle after applying a known load to the system [8]. However, this approach was not possible with our robot arm because of the limitations of hardware access by the manufacturer of the Mitsubishi PA-10 robot arm. We were therefore forced to characterize the stiffness characteristics in terms of measurable parameters such as input torque and motor axis position.

To observe the effect of HDT compliance on the performance of the Mitsubishi PA-10 robot arm, we performed a set of experiments in which the joints of the robot were commanded to follow a trajectory from -90° (maximum gravity torque) to 0° (fully upright) to $+90^\circ$ (minimum gravity torque) in velocity mode. The robot was mounted on the wall for joints 1, 3, and 5, and mounted on the pedestal for joints 2, 4, and 6. The purpose of these experiments was to observe the behavior of the joints under varying load conditions. A plot of the joint torque required to follow the trajectory for joint 2 is shown in Fig. 7(a) (total-feedback torque). Note the sharp decrease in torque when the output torque approaches 0 N · m (low-stiffness region). To verify that this behavior consistently occurs when the output torque approaches 0 N · m, we repeated the experiments for each joint with weights from 0 to 4.5 kg attached to the end-effector. In our experimental results, we observed that this sharp decrease in torque did occur consistently as the load on the joint approached 0 N · m [7]. This could be attributed to the soft wind-up behavior of the harmonic drive system. As the load on the wave generator decreased, the stiffness of the wave generator decreased, hence more torque output was required to sustain motion.

We determined the torque used to deform the compliant elements of the HDT by sequentially subtracting each of the components of the total torque required to produce the motion in Fig. 7(a). In our model of the HDT, the total torque required to produce the motion was composed of friction torque (static and viscous), gravity torque, and the torque used to deform the HDT. Therefore, after subtracting the known values of friction torque and gravity torque from the total torque, the remaining torque was assumed to be the torsional torque [(5)]. The friction torque was nearly identical with the coulomb friction, hence we could eliminate friction by subtracting the coulomb friction torque from the total torque (as noted previously, coulomb friction

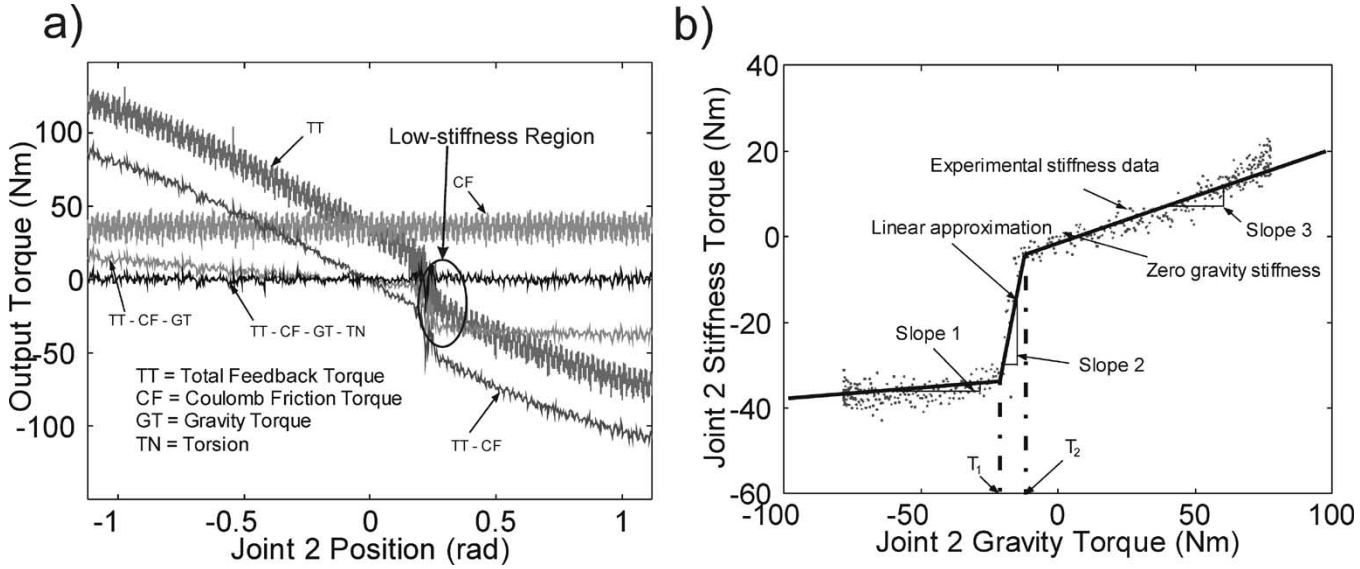

Fig. 7. (a) Steps in model identification process for joint 2. (b) Stiffness torque as a function of gravity torque in positive direction for joint 2.

torque was computed from the arm motion at low velocity while it was attached to the wall). The gravity torque was also known from the estimated masses of the robot arm links and the known weights attached to the robot. We could therefore subtract the gravity torque from the right side of (5). This left the remaining torque equal to the torque used to deform the wave generator.

Fig. 7(a) shows the results of each of the successive subtraction steps in determining the parameters of the HDT model for joint 2. The resulting torque after subtracting all the model components is shown in Fig. 7(a), and in the ideal case this torque should be zero over the entire range of motion for a given joint. As shown in Fig. 7(a), this torque was nearly zero except at points where the joint passed through a region of low HDT stiffness (gravity and friction approached equilibrium at these points). This effect was noticeable in all four joints and was partially caused by the kinematic error in the HDT. The sinusoidal torque transmitted to the joint was no longer approximated well by our coulomb friction model in this region because of the decreased stiffness of the HDT. The result was a sinusoidal error in our model that was essentially an error in approximating the amplitudes of the torque transmitted to the joint through the HDT, which were significantly lower in the low-stiffness region of the HDT. To accurately model this effect, a measurement of output axis rotation (i.e., output of the HDT) is required. This was not possible, however, with the current Mitsubishi PA-10 robot arm control architecture. If newer versions of the Mitsubishi PA-10 robot arm allow access to this value, our methodology could be straightforwardly extended to generate a more accurate model.

The remaining task was to determine how best to model the torque used to deform the wave generator. This is typically accomplished by measuring the wave generator angle and the output angle and by determining the deflection in the wave generator using (2). However, because of the limitation of hardware access of the Mitsubishi PA-10 robot arm, we were forced to model this torque with measurable parameters, i.e., the motor torque or motor position. Because wave generator deformation must be a function of the load on the system, we chose to model this torque as a function of the gravity torque and friction torque. Based on our experimental observation, the torque used to deform the wave generator was modeled as comprising of three linear regions for each direction of motion. For the feedforward implementation, we used the data collected in the previous experiments to generate a relationship between the gravity torque (which represents the external load on the joint during free motion) and the torque required to deform the compliant elements of the HDT. The nonlinear input-output relationship was again modeled as three linear regions. Fig. 7(b) shows the experimental stiffness data for joint 2 along with the linear approximations for each of the three regions. The parameters for joints 1 through 4 are given in Table V for both the positive and negative directions, including the slopes of each of the three linear regions, the transition points for the linear regions, and the value for stiffness when the external torque is zero.

We are presenting only the results of joints 1 through 4 in this section because they are the only joints that are significantly affected by gravity and the nonlinear stiffness of the HDT. Joints 1 through 4 experience a very low external load when the gravity and friction effects approach equilibrium, and consequently experience very low stiffness in the HDT. For the remaining joints (5, 6, and 7), the gravity torque was never large enough to balance the friction torque during free motion. These joints therefore never experienced the nonlinear effects of HDT compliance.

V. Experimental Verification of the HDT Model

To verify our model-based controller for the Mitsubishi PA-10 robot arm, we fed forward the torques computed by our model to track an end-effector trajectory with the robot in torque mode. The chosen trajectory was a lemniscate in the y-z plane of the

TABLE V
PARAMETERS FOR NONLINEAR STIFFNESS AS A FUNCTION OF GRAVITY TORQUE FOR JOINTS 1 THROUGH 4 FOR BOTH THE POSITIVE AND NEGATIVE DIRECTIONS

Joint	Slope 1 (N•m/N•m)	T_1 (N•m)	Slope 2 (N•m/N•m)	T_2 (N•m)	Slope 3 (N•m/N•m)	Zero-gravity stiffness (N•m)
Joint 1 +ve	–0.0044	–25.36	2.33	–12.70	0.26	2.32
Joint 1 –ve	0.04	12.16	–1.93	19.53	–0.34	0.19
Joint 2 +ve	0.31	–23.48	2.63	–11.75	0.20	–1.44
Joint 2 –ve	–0.06	11.16	–2.80	21.75	–0.27	0.45
Joint 3 +ve	0.21	–5.78	4.26	–3.49	0.09	0.81
Joint 3 –ve	0.02	5.30	–3.60	2.64	–0.07	–0.30
Joint 4 +ve	0.22	–19.58	5.08	–16.27	0.92	2.57
Joint 4 –ve	–0.68	15.14	–4.11	19.23	–0.18	–1.45

base coordinate system. This trajectory was chosen because the joint velocities for the trajectory were within the regions that we have modeled, thereby providing us with the necessary data to validate our estimation and modeling approach. The expression for this trajectory is given by:

$$x = 0.6, \quad y = 0.2\frac{\cos\left(\frac{t}{2}\right)}{\left(1+\sin\left(\frac{t}{2}\right)^2\right)}$$

$$z = 0.1 + 0.4\frac{\sin\left(\frac{t}{2}\right)\cos\left(\frac{t}{2}\right)}{\left(1+\sin\left(\frac{t}{2}\right)^2\right)}. \tag{14}$$

The end-effector position followed the lemniscate position, whereas the end-effector orientation remained constant relative to the base coordinate system. We computed the necessary joint angles for this trajectory by using the kinematic parameters and inverse kinematics solution for six joints. The results of the end-effector trajectory-tracking experiments are shown in Fig. 8. The mean end-effector error was 7 mm, with a maximum error of 42 mm occurring at the beginning of the experiment. After the initial large error, the maximum tracking error was 19 mm. The proportional and derivative gains for this experiment are shown in Table VI. The velocity of robot joints was estimated using a Butterworth filter with a cutoff frequency of 200 Hz. This filter was chosen because it was empirically determined to give the best results. In our feed-forward implementation, we used the filtered velocity for the derivative error torque and we used the desired velocity for friction and stiffness torque.

Fig. 9 shows the individual torques required follow the desired trajectory for each joint. If our model of the harmonic drive transmission was accurate, then low-feedback torques would be required to track the desired trajectory [6]. The figures for joints 2 and 4 include the full harmonic drive transmission model described by (5), i.e., friction torque (position-dependent plus velocity-dependent friction torque), gravity torque, stiffness torque, and feedback torque. The model for joint 1 includes only friction torque and feedback torque because there was no gravity or nonlinear stiffness effect for joint 1 because the robot was mounted on the pedestal. The figures for joints 5, 6, and 7 also show only friction torque and feedback torque because joint 7 experienced no gravity or nonlinear stiffness effects, and joints 5 and 6 experienced gravity effects that were small compared with friction (the maximum gravity torque for each joint was approximately 0.3 N · m). As seen from Figs. 8 and 9, our

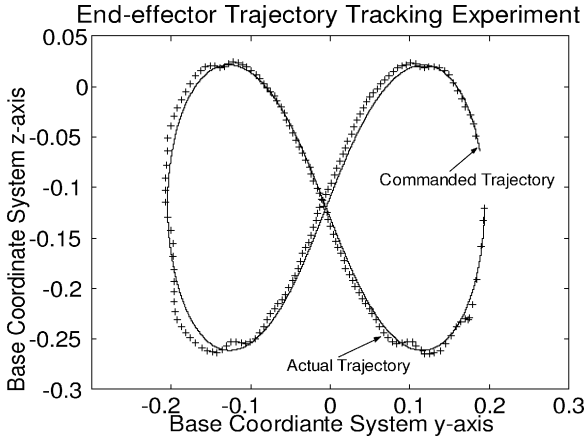

Fig. 8. End-effector trajectory-tracking experiment.

TABLE VI
PROPORTIONAL AND DERIVATIVE GAINS FOR END-EFFECTOR TRAJECTORY-TRACKING EXPERIMENT

Joint	Proportional Gain (N•m/rad)	Derivative Gain (N•m/rad/s)
1	4.0	1.0
2	5.0	1.0
4	2.0	0.5
5	0.6	0.05
6	1.2	0.15
7	0.6	0.05

estimation and modeling approach for the various components of the Mitsubishi PA-10 robot arm for low-velocity trajectory tracking was successful.

A. Experimental Results for Joint 3

In the experiment described above, joint 3 was locked to simplify the inverse kinematics calculations required to track the desired trajectory. To demonstrate the implementation of our model for joint 3, we performed an additional experiment in which joint 3 was commanded to follow a trapezoidal velocity profile, whereas the torques computed from our model were fed forward to the joint. This experiment was performed in torque mode with the robot mounted on the pedestal. The robot was configured so that the trajectory began with a maximum load due to gravity on the joint. The robot was then commanded to move a distance of 1.0 rad at a speed of 0.1 rad/s. The torques required

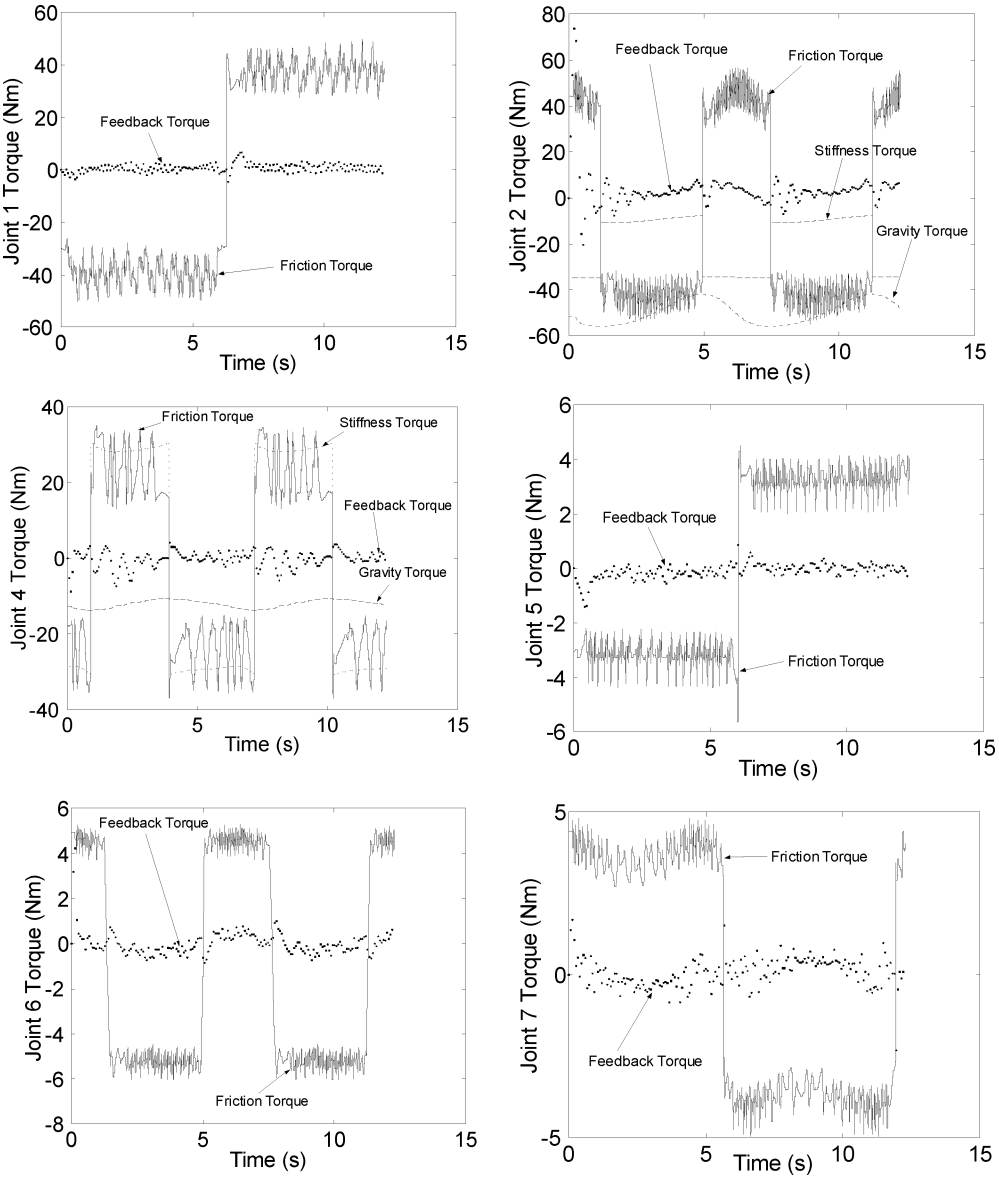

Fig. 9. Individual joint torques during trajectory-tracking experiment.

to complete this motion are shown in Fig. 10. In this experiment, the proportional gain was 4.0 N · m/rad, the derivative gain was 0.5 N · m/rad/s, and the mean error for tracking the trajectory was 0.01 rad.

VI. Discussion

In this paper, we have presented our approach for developing a model-based controller through careful experimental determination of the dynamic model for the HDT in the Mitsubishi PA-10 robot arm. We first developed a mathematical model for the HDT accounting for friction, transmission compliance, and gravity. For each of these terms, the model parameters were based on observed experimental data. We then fed forward our model to the robot for the purpose of tracking a desired trajectory to demonstrate the performance of our model-based controller

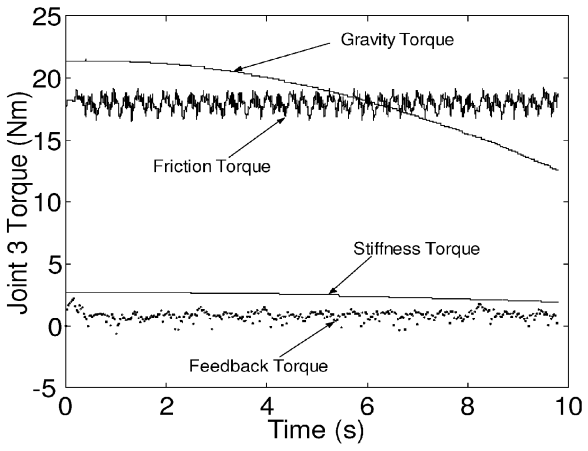

Fig. 10. Computed torques for joint 3 while monitoring a trapezoidal velocity profile.

and the accuracy of our estimation and modeling approach. The success of our model implementation was demonstrated by the ability of the robot to track a trajectory with reasonable accuracy by using low-feedback gains. Using these low-feedback gains without our feedforward model would cause the robot to collapse under its own weight. Furthermore, achieving the same accuracy in trajectory tracking without our model would require increasing the feedback gains used in our experiment by at least a factor of 10.

One of the most challenging aspects of modeling the harmonic drive transmission in the Mitsubishi PA-10 robot arm was effectively modeling the effects of nonlinear stiffness. Our approach for modeling the nonlinear stiffness was to model the torque required to deform the compliant elements of the transmission as a function of the external load on the transmission (which is the gravity torque in the case of free motion). To model the nonlinear stiffness in a form that can be implemented in a feedforward model, we quantified the relationship between the torque used to deform the wave generator and the gravity torque. We have experimentally determined separate parameters for the stiffness torque when the joint is moving in the positive and negative directions. Recall that our definition of coulomb friction is the torque required to maintain a very slow velocity of the range of motion of the joint. Therefore, the effect of wave generator deformation has already been accounted in our friction model for a given direction. Wave generator compliance gives the appearance of coulomb friction and backlash because of the soft wind-up properties of the harmonic drives. Because the nonlinear stiffness behavior of the wave generator occurs only in a narrow region of low applied torques (lower than the torque required to initiate motion), its effect is not noticeable at higher applied loads. Therefore, the effect of low wave generator stiffness is only significant when the gravity torque and friction torque approach a point of static equilibrium. This situation only occurs for joints 1 through 4 during free motion and depends on the robot configuration.

In the experimental verification of our model, we used low-feedback gains to track a desired end-effector trajectory. Although, in general, our model performed well, our control methodology does result in tracking errors in areas of very low velocity (<0.1 rad/s) and in velocity reversals. The low-velocity tracking errors could in part be explained by our method of feeding forward the friction torque to our controller. We fed forward friction torque based on the desired joint velocity as opposed to the actual joint velocity. We chose this method to feed forward friction torque because we did not have a reliable means of estimating velocity. Our velocity measurements were made by differentiating and filtering position measurements, which resulted in a noisy velocity measurement. Using these noisy velocity measurements in the feed-forward implementation of our controller resulted in a behavior similar to the "stick-slip" situation and significantly degraded the performance of the controller. We experimented with several filtering schemes for the position measurements and concluded that the best results were obtained by using the desired velocity in our feed-forward implementation. Although this method provided the best results in our case, it is generally preferable to use the actual joint velocity for feed-forward friction torque if a reliable velocity measurement is available. This was demonstrated by Johnson and Lorenz in [22], where it was shown that feeding forward the friction torque based on the actual joint velocity performed better than the desired joint velocity, especially for low velocities. We therefore see the lack of reliable velocity estimation as a limitation to our control method because of inaccurate measurements of velocity reversals and degraded performance of the controller at low velocities. However, newer versions of the Mitsubishi PA-10 robot arm include a velocity measurement in the servo driver. Hence, the implementation of our control scheme on future Mitsubishi PA-10 robot arm models will benefit significantly from these velocity measurements.

If our model were perfect, we should expect to see zero-feedback torque required to follow a desired trajectory. In our experimental results, the feedback torques were lowest in regions where the desired joint velocities were greater than 0.1 rad/s, and highest in regions of lower velocity and velocity reversals. Joints 2 and 4 demonstrate the results of our complete model, because the remaining joints include only friction and feedback torque. In the controller implementation for joints 2 and 4, a velocity reversal entails a switch in direction for both friction and stiffness torque. Therefore, accurate modeling of both friction and stiffness are essential in regions of velocity reversal. The high-feedback torques in regions of velocity reversal are thus partially explained by inaccuracies in estimating the stiffness torque for a given joint configuration. In our previous work [7], we demonstrated the decreased performance of our controller in regions of "low wave generator stiffness", when friction and gravity torque approach a state of equilibrium. This resulted in a very low load on the HDT. Our test trajectories in this paper simply avoided regions of low wave generator stiffness, which was fairly straightforward for a free-motion experiment, because these regions occur at predictable points where the gravity torque equals the friction torque. To accurately compensate for the effect of nonlinear stiffness in the HDT, a measurement of output joint position is required. If measurement of the joint torsion angle was possible, the catalog values of the HDT stiffness could be used in the feed-forward controller to accurately determine the stiffness torque.

VII. Summary and Conclusions

We have presented our research on developing a dynamic model of the HDT in the Mitsubishi PA-10 robot arm for low-velocity applications by using low-feedback gains. A model of the HDT was developed that successfully allowed low-velocity trajectory tracking outside the region of low wave generator stiffness. Although our controller performed fairly well for each joint of the robot, the performance of our control methodology could be significantly improved by a reliable measurement of joint velocity and a measurement of the torsion angle for each joint. These improvements would allow for better low-velocity trajectory tracking, better performance of the controller near velocity reversals, and accurate estimation of the torque required to deform the compliant elements of the HDT. The Mitsubishi PA-10 robot arm is widely used in research laboratories worldwide,

yet no published work addresses the modeling of the dynamic properties of the HDT for every joint of the robot. Despite the limitations of hardware access in the current Mitsubishi PA-10 robot arm, we believe that the methodology presented in this paper will benefit the research community using this robot arm.

REFERENCES

[1] C. W. Kennedy and J. P. Desai, "A novel approach to robotic cardiac surgery using haptics and vision," *Cardiovasc. Eng. Int. J.*, vol. 2, no. 1, pp. 15–22, 2002.

[2] ——, "A vision-based approach for estimating contact forces: Applications to robot-assisted surgery," in *J. Appl. Bionics and Biomech.*, to be published.

[3] Y. Hirata, T. Takagi, K. Kosuge, H. Asama, H. Kaetsu, and K. Kawabata, "Manipulation of a large object by multiple DR helpers in cooperation with a human," in *Proc. IEEE/RSJ Int. Conf. Intell. Robots Syst.*, 2001, pp. 126–131.

[4] W. K. Yoon, Y. Tsumaki, and M. Uchiyama, "An experimental system for dual-arm robot teleoperation in space with concepts of virtual grip and ball," in *Proc. Int. Conf. Advanced Robotics*, 1999, pp. 225–230.

[5] M. M. Olsen and H. G. Peterson, "A new method for estimating parameters of a dynamic robot model," *IEEE Trans. Robot. Autom.*, vol. 17, no. 1, pp. 95–100, Feb. 2001.

[6] J. P. Desai and R. D. Howe, "Towards the development of a humanoid arm by minimizing interaction forces through minimum impedance control," in *Proc. IEEE Int. Conf. Robotics Autom.*, 2001, pp. 4214–4219.

[7] C. W. Kennedy and J. P. Desai, "Estimation and modeling of the harmonic drive transmission in the Mitsubishi PA-10 robot arm," in *Proc. IEEE/RSJ Int. Conf. Intell. Robots Syst.*, 2003, pp. 3331–3336.

[8] T. D. Tuttle, "Understanding and modeling the behavior of a harmonic drive gear transmission," M.S. thesis, MIT Artif. Intell. Lab., Cambridge, MA, 1992.

[9] N. Kircanski and A. A. Goldenberg, "An experimental study of nonlinear stiffness, hysteresis, and friction effects in robot joints with harmonic drives and torque sensors," *Int. J. Robot. Res.*, vol. 16, no. 2, pp. 214–239, 1997.

[10] H. D. Taghirad, "On the modeling and identification of harmonic srive systems," Tech. Rep. CIM-TR-97-02, McGill Univ., Centre for Intelligent Machines, Montreal, QC, Canada, Jan. 1997.

[11] I. Godler, T. Ninomiya, and M. Horiuchi, "Ripple compensation for torque sensors built into harmonic drives," *IEEE Trans. Instrum. Meas.*, vol. 50, no. 1, pp. 117–122, Feb. 2001.

[12] M. Hashimoto,, T. Shimono, K. Koreyeda, H. Tanaka, Y. Koyosawa, and H. Hirabayashi, "Experimental study on torque control using harmonic drive built-in torque sensors," in *Proc. IEEE Int. Conf. Robotics Autom.*, 1992, pp. 2026–2031.

[13] H. D. Taghirad and P. R. Belanger, "Torque ripple and misalignment torque compensation for the built-in torque sensor of harmonic drive systems," *IEEE Trans. Instrum. Meas.*, vol. 47, no. 1, pp. 309–315, Feb. 1998.

[14] W. Khalil and S. Besnard, "Geometric calibration of robots with flexible joints and links," *J. Intell. Robots Syst.*, vol. 34, no. 4, pp. 357–379, 2002.

[15] T. Tsumugiwa, R. Yokogawa, and K. Hara, "Measurement method for compliance of vertical-multi-articulated robot: Application to 7-DOF robot PA-10," in *Proc. IEEE Int. Conf. Robotics Autom.*, 2003, pp. 2741–2746.

[16] M. Itoh, "Suppression of transient vibration for geared mechanical system using model-based control," in *4th Int. Conf. Motion Vibration Control*, 1998, pp. 328–335.

[17] H. D. Taghirad and P. R. Belanger, "Robust torque control of harmonic drive under constrained-motion," in *Proc. IEEE Int. Conf. Robotics Autom.*, 1997, pp. 248–253.

[18] M. M. Moghaddam and A. A. Goldenberg, "Nonlinear modeling and robust H-infinity based control of flexible joint robots with harmonic drives," in *Proc. IEEE Int. Conf. Robotics Autom.*, 1997, pp. 3130–3135.

[19] A. Timcenko and N. Kircanski, "Control of robots with elastic joints: Deterministic observer and Kalman filter approach," in *Proc. IEEE Int. Conf. Robotics Autom.*, 1992, pp. 722–727.

[20] B. Armstrong-Helouvry, *Control of Machines with Friction*. Norwell, MA: Kluwer, 1991.

[21] T. W. Nye and R. P. Kraml, "Harmonic drive gear error: Characterization and compensation for precision pointing and tracking," in *Proc. 25th Aeros. Mechanisms Symp.*, 1991, pp. 237–252.

[22] C. T. Johnson and R. D. Lorenz, "Experimental identification of friction and its compensation in precise, position controlled mechanisms," *IEEE Trans. Ind. Appl.*, vol. 28, no. 6, pp. 1392–1398, Nov./Dec. 1992.

Christopher W. Kennedy (S'05) received the B.S., M.S., and Ph.D. degrees in mechanical engineering from Drexel University in 2001, 2003, and 2004, respectively.

Since 2004, he has been a Postdoctoral Fellow at the Engineering Research Center for Computer-Integrated Surgical Systems and Technology at Johns Hopkins University. His current research interests include medical robotics, visual-servoing, and model-based control of robotic systems.

Jaydev P. Desai (S'97–M'97–A'98) received the M.S. degree in mechanical engineering and applied mechanics, the M.A. degree in mathematics, and the Ph.D. degree in mechanical engineering and applied mechanics, from the University of Pennsylvania in 1995, 1997, and 1998, respectively. He completed his undergraduate studies from the Indian Institute of Technology, Mumbai, India, in 1993.

He is currently an Assistant Professor in the Department of Mechanical Engineering and Mechanics at Drexel University and the Director of the Program for Robotics, Intelligent Sensing, and Mechatronics (PRISM) Laboratory. He is also an Adjunct Assistant Professor in the Department of Cardiothoracic Surgery at Drexel University College of Medicine. Prior to joining Drexel University in the Fall of 1999, he was a Post-Doctoral Fellow in the Division of Engineering and Applied Sciences at Harvard University.

Dr. Desai is a recipient of the 2002 NSF CAREER award and the 2004 Ralph R. Teetor Educational Award. His research interests include medical robotics, reality-based modeling of soft tissue interaction for surgical simluation, model-based teleoperation, and modeling and control of robot manipulators. He is also a Member of the ASME.